C_2F, BN, and C nanoshell elasticity from *ab initio* computations

Konstantin N. Kudin and Gustavo E. Scuseria
Department of Chemistry, Rice University, Houston, Texas 77005-1892

Boris I. Yakobson
Department of Mechanical Engineering and Materials Science, Rice University, Houston, Texas 77005-1892

(Received 15 June 2001; revised manuscript received 2 August 2001; published 15 November 2001)

Two-dimensional lattices of carbon, boron-nitride, and fluorine-carbon compositions are treated with *ab initio* methods in order to evaluate and compare their mechanical properties in a uniform fashion. The demonstrated robustness of continuum elasticity up to very small length-scale allows one to define and compute the in-plane stiffness and flexural rigidity moduli of the representative nanoshells of C, BN, and C_xF ($x \leqslant 2$). While only small deviations from linear elasticity are observed for C and BN, fluorination causes significant spontaneous shell folding. We discover that spontaneous curvature in fluorinated nanotubes shifts the energy minimum from a plane sheet towards the very small diameter tubes of (4,4) and even (3,3) indexes. Moreover, their equilibrium cross sections are distinctly polygonal, due to curvature self-localization, with an equilibrium angle of 71° at each fluorine row attachment. Our analysis yields a simple physical model coupling the mechanical strain with chemical transformation energies.

DOI: 10.1103/PhysRevB.64.235406 PACS number(s): 71.20.Tx

I. INTRODUCTION

With the discovery of hollow molecular structures like fullerene cages[1] and especially single-wall nanotubes,[2–5] it has been demonstrated that their nonlinear mechanical and certain vibration properties can be well described in terms of a continuum model, nanoshell of a monatomic thickness, or an array of such layers.[6–8] The shell approach essentially ignores the explicit atomic structure and requires no detailed knowledge of interatomic forces.[9] But it must be supplied with the appropriate accurate values of the shell stiffness, that can be obtained from *ab initio* methods, since no experimental measurements are currently feasible.

The hexagonal symmetry of pure C and BN two-dimensional lattices ensures their isotropic elastic properties and thus justifies an isotropic shell model,[6,8,10] characterized by only three elastic parameters. This is not the case for C_2F and other C_xF lattices that permit a variety of decorations of different symmetry. Moreover, this anisotropy manifests itself even in the equilibrium shape of C_xF tubules as we will see below. As soon as a plane or a nanotube-forming monatomic layer is approximated by a continuum isotropic shell, its deformation energy U can be written down in standard form, as a function of in-plane strain ϵ and the changes of curvatures κ in two orthogonal directions, x in axial and y in circumferential[10]

$$U=\frac{1}{2}\int\int\left\{D[(\kappa_x+\kappa_y^2)-2(1-\nu)(\kappa_x\kappa_y-\kappa_{xy}^2)]+\frac{C}{(1-\nu^2)}[(\epsilon_x+\epsilon_y)^2-2(1-\nu)(\epsilon_x\epsilon_y-\epsilon_{xy}^2)]\right\}dS. \tag{1}$$

Here C, ν, and D are the in-plane stiffness, Poisson ratio, and flexural rigidity for the continuum shell. These are the parameters to be evaluated based on *ab initio* energy calculations. Clearly, energy as a function of elongation in a simple tension (that is unconstrained laterally or in any other way) should yield the value of C. Indeed, in this case tension ϵ_x causes the diameter or circumference reduction $\epsilon_y=-\nu\epsilon_x$, so that $U=\frac{1}{2}C\epsilon_x^2$. The value of ν can be evaluated from the actual reduction of diameter in the same samples. The value of flexural rigidity D can be defined as a coefficient in energy of unloaded/free relaxed tubule as a function of its diameter d: $U=\frac{1}{2}D\kappa_x^2=2D/d^2$.

Unlike more common material moduli, C has dimensionality of surface tension N/m and can be defined in terms of measurable characteristics of a nanotube

$$C=\frac{1}{L}\frac{\partial^2 U}{\partial\epsilon^2}\frac{1}{\int dl}=\frac{1}{a}\frac{\partial^2 E}{\partial\epsilon^2}, \tag{2}$$

where E is the strain energy computed per atom, and $a=m/\rho_s$ is the area per atom in a two-dimensional (2D) lattice, related with the 2D mass density ρ_s and the mass of atom m. The partial derivative at zero strain in all dimensions except ϵ yields an analog of the elastic stiffness C_{11} in graphite, while a free boundary (no lateral traction on nanotube) would correspond to the Young's modulus $Y=S_{11}^{-1}$ (S_{11} being the elastic compliance). In an *array* of tubes, if the material is distributed statistically uniformly over a large cross section A (perpendicular to the generatrix) with the bulk density ρ_b, the Young's modulus can be recovered and used,

$$Y=C\int\frac{dl}{A}=C\frac{\rho_b}{\rho_s}=\frac{\rho_b}{m}\frac{\partial^2 E}{\partial\epsilon^2}. \tag{3}$$

These definitions do not apply in case of individual shell or a single nanotube, due to uncertainty of either cross section A,

bulk density ρ_b, or an arbitrary geometrical thickness h in a relationship $Y=C/h$. However, continuum shell can be assigned the modulus Y_s and thickness h unambiguously, to formally match the ν, C, and D, computed *ab initio*:

$$C=Y_s h \quad D=\frac{Y_s h^3}{12(1-\nu^2)}. \tag{4}$$

In the following sections, we outline the computational approach (Sec. II), including some of the observed aspects of the electronic structure, in order to illustrate consistency of the method. Then we present the mechanical parameters computation, comparing with previously published results wherever appropriate. Axial tension produces values for the in-plane stiffness C and Poisson ratio ν, for all-carbon, boron-nitride, and fluorinated-carbon shells (Sec. III). Comparisons of the energies of the nanotubes of different diameters yields the values for flexural rigidity D in Sec. IV, where we also note the spontaneous curvature of fluorinated shells. This leads to an interesting observation in Sec. V about strain localization, when the shell curvature is concentrated at the F-attachment sites rather than remaining uniformly distributed along the circumference. As a result, the equilibrium cross section of nanotubes becomes distinctly polygonal, with triangle and square shapes as most favorable. In the concluding Sec. VI, we apply the *ab initio* values of C, D, and ν (or alternatively of h, Y_s, and ν) to estimate basic vibration frequencies and buckling stability limits of the nanotubes.

II. COMPUTATIONAL DETAILS

A. Methodology

To carry out the present calculations, we employ the implementation of density functional theory with Gaussian type orbitals and periodic boundary conditions[11] (PBC) recently incorporated into the development version of the GAUSSIAN suite of programs.[12] The PBC code evaluates the Kohn-Sham matrix contributions entirely in direct space, and the computational expense for these parts of the calculation scales linearly $[O(N)]$ with system size. The matrix operations in reciprocal space, such as the diagonalization of **k** point dependent Kohn-Sham matrices, requires CPU time that scales cubically $[O(N^3)]$ with the number of basis functions N. Their absolute cost is such that for the largest systems considered here (160 atoms, 1440 basis functions), these $O(N^3)$ operations become similar in cost to the $O(N)$ Kohn-Sham matrix formation step. For reference, one full geometry optimization step (12 SCF cycles for an energy calculation and a gradient evaluation without employing any spatial symmetry) for (40,40) BN tube takes about 90 h on one R10000 195 Mhz CPU of SGI Origin 2000, out of which about 60 h are spent for $O(N^3)$ matrix computations (16 diagonalizations per cycle). The use of Gaussian basis sets permits sufficient flexibility in the description of both valence and core electrons for elements across the first half of the periodic table and keeps the number of basis functions per atom small.

From the multitude of available density functional models, we have chosen the gradient corrected PBE functional derived by Perdew, Burke, and Ernzerhof.[13] Calculations with the PBE functional have computational cost similar to other gradient corrected functionals, while providing more consistent results for a variety of chemical systems.[13] Combining the PBE functional with the double zeta quality 3–21 G basis set, we expect to obtain a theoretical model capable of providing very good description of the various mechanical properties studied in this work.

The Coulomb interactions in the code are evaluated via the fast multipole method[14] with an accuracy within 10^{-9} atomic units (a.u.).[11,15–18] The numerical integration of the exchange-correlation energy and potential employs atomic centered grids. In most calculations, the (75,302) integration grid was used, which corresponds to the default grid in the GAUSSIAN package. In computations where small differences in energy and geometry were of great importance, such as in-plane stiffness and Poisson ratios, the *ultrafine* grid was used (99 radial and 590 angular points). In order to achieve good convergence in reciprocal space integration for SWNT's, we employed 32 **k** points for insulators and 128 **k** points for metallic systems. In the latter case, to obtain smooth changes in SWNT's geometries under small strains and accurate Poisson ratios, we determined the exact location of the Fermi level in **k** space and employed this information to compute correct weights for orbitals located close to the crossing of the energy bands at the Fermi level. In 2D structures, a mesh of **k** points was employed with 64 points along the shorter translational vector and the proportionally smaller number along the longer vector.

Full geometry optimizations were carried out by a recently developed redundant internal coordinate method,[19] where the lattice vectors are optimized implicitly via a combination of intercell bonds, valence angles, and dihedrals. At each optimization step, the unit cell symmetry was enforced in order to suppress small numerical noise in forces due to the imperfect rotational symmetry of the angular grids. Accordingly, in each case the atomic arrangement in unit cells was chosen such as to maximize the symmetry. The optimizations were stopped when the r.m.s of forces was below 0.0003 a.u. (0.015 eV/Å), and the r.m.s. of Cartesian displacements was below 0.0012 a.u. (0.0006 Å).

In the calculations of the in-plane stiffness and the Poisson ratio, fully optimized structures of smaller radius tubes were stretched by $\pm 0.3\%$ and $\pm 0.6\%$. For larger diameter tubes, we applied strains of $\pm 0.3\%$ only, because in smaller diameter tubes such strains were sufficiently reliable to obtain the desired precision. During reoptimizations under strain, the lattice vectors were kept fixed, while all the other parameters were relaxed. This was achieved via the facility to constrain some coordinates in the redundant internal coordinate algorithm for periodic systems.[19] To achieve very high accuracy, the optimization thresholds were tightened up to r.m.s. of forces of 0.00001 a.u. (0.0005 eV/Å) and r.m.s. of Cartesian displacements of 0.00004 a.u. (0.00002 Å).

In studies of achiral zigzag $(n,0)$ and armchair (n,n) nanotubes, the unit cell under consideration contained $4n$ atoms regardless of the tube type. For 2D structures, we em-

TABLE I. Predicted elastic constants for carbon nanotubes from periodic PBE/3-21G calculations.

Tube	$d^2E/d\epsilon^2$	C,J/m^2	ν	$\frac{1}{6}d^3E/d\epsilon^3$	R	L_1	L_2
(4,4)	56.4	333	0.144	−90	2.7859	2.4772	
(7,0)	56.3	333	0.162	−310	2.8157		4.2882
(7,7)	56.5	338	0.146	−70	4.8154	2.4783	
(12,0)	55.2	330	0.181	−260	4.7678		4.2917
graph (∞,∞)	57.3	345	0.149	−240		2.4795	
graph (∞,0)	57.3	345	0.149	−170			4.2945

ployed rectangular unit cells, which had four atoms in the unit cell. Fluorinated carbon tubes discussed in this work also contained $4n$ carbon atoms in the unit cell plus the necessary number of fluorines.

B. Electronic structure

In this work, we look at a series of achiral zigzag $(n,0)$ and armchair (n,n) single-wall nanotubes (SWNT). The n values we chose were 3, 4, 5, 6, 8, 10, 12, 14 and also 20, 28, and 40 for armchair BN tubes. We have also considered the structures with effective $n=\infty$–graphite and planar BN. The electronic structure of the carbon SWNT's (CNT's) was found to be in agreement with previous calculations at lower levels of theory.[20,21] All CNT's of the (n,n) chirality were metallic, while larger diameter $(n,0)$ tubes were either moderate gap or narrow gap semiconductors, with the latter type of behavior found for structures where n was a multiple of 3.[20] Small diameter $(n,0)$ tubes were metallic up to $n=6$ due to the substantial curvature, in agreement with the results of others.[21] Recently, we have found that the (5,0) tube distorts to elliptic shape and becomes semiconducting,[11] lowering its energy and symmetry. Here, we neglect this subtle effect and consider only the cylindrically symmetric (5,0) structure for consistent comparison with other tubes that are cylindrical at the minimum.

On the other hand, all BN SWNT's (BNNT's) had significantly larger band gaps. In armchair (n,n) BNNT's, the smallest band gap (4.1 eV) was obtained for the (3,3) BNNT, and this value rapidly increased to the 4.5 eV gap of planar BN, reaching it in (5,5) BNNT. At the same time, in zigzag $(n,0)$ structures, the smallest band gap of 1.2 eV found in (3,0) BNNT increased more slowly with n and reached the planar BN value only at about $n=14$. While the trends for band gaps found in our BNNT calculations agree qualitatively with the previous tight-binding studies,[22] we find that the latter calculations underestimate the band gap for smaller radius BNNT's compared to our results, while for larger BNNT's the values are in good agreement. On the other hand, LDA calculations[23] predict the band gap for (4,4) BNNT to be close to the gap of planar BN sheet, similar to what we see in our calculations.

In our recent work, we studied various isomers of fluorinated CNT's (F-CNT's) with C_2F stoichiometry.[24,25] Calculations for (10,10) and (18,0) tubes with approximately matching radius have demonstrated that among all (10,10) and (18,0) F-CNT's, the energy per C_2F unit is the lowest for all fluorine outside isomers in (10,10) fluorinated nanotube with zigzag chains of fluorine atoms located parallel to the tube axis. Therefore, here we look at the series of (n,n) F-CNT's with the same fluorination pattern. We fully optimized F-CNT's of (n,n) with $n=3,4,5,6,8,10,12$, as well as the corresponding 2D structure $(n=\infty)$. We have also considered (12,12) F-CNT's with fluorine chains inside the tube that formally corresponds to negative curvature. F-CNT's with all outside fluorines are metallic with varying number of crossings at the Fermi level, indicating the presence of significant interaction between polyacetylene-like sp^2 carbon chains separated by chains of fluorinated sp^3 carbon. The alternation of conjugated bonds (Peierls instability) is unable to open the gap and lower the energy, and therefore the length of these bonds remain identical. The fluorination also causes significant distortions in the tube framework, with sp^2 carbons located closer to the tube axis than sp^3 carbons (a result of localized curvature, ''pinch'' effect as discussed in Sec. IV C).

III. IN-PLANE STIFFNESS C, AND POISSON RATIO ν

By performing an extension of the tubes, we calculated the $d^2E/d\epsilon^2$ values and the Poisson ratio for pairs of tubes of similar radius but different helicity. The former can be readily recomputed into the usual Young moduli, following equations (2), (3). For both CNT's and BNNT's, the pairs were (4,4) and (7,0) and (7,7) and (12,0). For comparison purposes, the corresponding values for the 2D structures were also calculated, and these formally correspond to $(\infty,0)$ and (∞,∞) types. The results for CNT's are shown in Table I and for BNNT's in Table II. Overall, there is no difference found in the $d^2E/d\epsilon^2$ values in neither carbon nor BN structures of varying radius. Slight variations appearing in Tables I and II are well within the error of the computational procedure. We estimate the error in the $d^2E/d\epsilon^2$ numbers to be of the order of 2%, while for Poisson ratios the errors are on the order of 0.5%. A similar situation was observed for CNT's in Ref. 26, where the differences between $d^2E/d\epsilon^2$ values for different CNT's are within the computational error. We also obtained estimates for the third derivative $d^3E/d\epsilon^3$ responsible for the anharmonicity in the energy versus strain curve dependence. For CNT's the $d^3E/d\epsilon^3$ values have the same sign, but are significantly different in magnitude. For BNNT's, on the other hand, the numbers are in much better agreement with each other. The difference between CNT's and BNNT's lies in their band gaps. While it is relatively easy to fully converge reciprocal space quantities

TABLE II. Predicted elastic constants for *BN* nanotubes from periodic PBE/3-21G calculations.

Tube	$d^2E/d\epsilon^2$	C,J/m^2	ν	$\frac{1}{6}d^3E/d\epsilon^3$	R	L_1	L_2	$R(N)$-$R(B)$
(4,4)	45.8	258	0.217	−450	2.8455	2.5490		0.0588
(7,0)	45.3	255	0.244	−420	2.8920		4.3906	0.0571
(7,7)	46.9	267	0.213	−370	4.9332	2.5441		0.0318
(12,0)	46.7	266	0.226	−310	4.8909		4.3999	0.0321
planar (∞,∞)	47.4	271	0.211	−250		2.5420		0
planar $(\infty,0)$	47.4	271	0.211	−250			4.4028	0

for large gap BNNT's, it is more challenging to do the same for CNT's that either have small gaps or are metallic.

Notably, the addition of a large number of fluorines to a carbon tube does not affect the stiffness of the carbon backbone, and fluorinated CNT $d^2E/d\epsilon^2$ values are similar to those found in pristine CNT's (Table III). At the same time, in C_2F tubes we observe much larger anharmonicity $d^3E/d\epsilon^3$, most likely due to the very short fluorine-fluorine distances (shorter than the sum of two van der Waals radii of fluorine). This indicates that fluorinated and other derivatized CNT's can be as stiff as the pristine nanotubes, and can be used in a variety of composite materials. Much larger anharmonicity, on the other hand, implies that under larger, greater deformations F-CNT's will be more compliant than pristine carbon tubes.

Poisson ratios for CNT's depend on the tube type and radius. The results for (n,n) structures seem to converge quite fast and the (7,7) tube results are already within 2% of the graphitic value of 0.149. The convergence is slower for $(n,0)$ structures. In fact when going from (7,0) to (12,0) CNT, the ratio changes in the other direction, from 0.162 to 0.181. Again, Poisson ratios computed by us are similar to the numbers from Ref. 26. In BNNT's, trends similar to carbon structures are observed. The Poisson ratios for (n,n) tubes converge faster to the planar BN value of 0.211 than for the $(n,0)$ structures. Comparing our data to the results of tight-binding calculations from Ref. 27, we note that the TB results are about 10% larger than the *ab initio* ones. This is a much smaller difference than for CNT's, where TB numbers are about 60% larger than *ab initio* ones.[27]

IV. FLEXURAL RIGIDITY D

A. Carbon tubes

An important characteristic of a 2D sheet of material is its flexural rigidity, i.e., the dependence of the strain energy on its curvature along some direction. By bending graphene or planar BN sheet, one obtains SWNT's of different chirality. Due to the hexagonal symmetry of both graphene and planar BN, there should be no difference in values of the D constant in Eq. (1) for tubes of varying chirality because these materials are isotropic. And indeed, our results for fully optimized tubes do confirm that there is no difference in strain energy for (n,n) and $(n,0)$ carbon and BN tubes except for the tubes of the smallest radii. Tube energy per atom relative to a flat graphene sheet is the same as the graphene sheet strain energy due to flexing, and is computed as $U(C) = [E_{\text{total}}(C) - \mu_C n_C]/n_C$. To analyze the dependence of the strain energy on tube radius (curvature) in more detail, we fit the data to equation $U = \frac{1}{2}D/R^a$. For carbon tubes, we find $a = 2.0$ with high precision. The value of the constant D determined from larger diameter CNTs is 3.9 eV Å^2/atom, and is independent of whether (n,n) or $(n,0)$ structures are considered. This number is in good agreement with the LDA-based values of 3.9 ± 0.1 eV Å^2/atom computed both for armchair and zigzag tubes,[28] and 4.00 eV Å^2/atom obtained from the pseudopotential-density-functional theory calculations for (n,n) tubes.[26] In the latter case, the authors have also obtained $D = 4.32$ eV Å^2/atom for the (10,0) structure, while in our calculations (and Ref. 28) no difference was found between (10,0) and a (n,n) CNT of matching radius. The lack of data for other $(n,0)$ CNTs in Ref. 26 does not allow us to make any statements about the nature of such a discrepancy. Figure 1 displays the strain energy as a function of the square of the inverse radius. Indeed, the data points for all tubes but the smallest ones, reside on the same line that goes through the point (0,0). The deviations observed for the smaller radii tubes on the left side in Fig. 1 disappear once the tube radius becomes larger than ~3 Å [(5,5) and (8,0) structures]. This is an indication that for a large range of curvatures, CNT's do behave as elastic shells.

B. BN tubes

In contrast to CNT's, both for zigzag and armchair *BN* tubes, we have found a slightly subquadratic dependence of the strain energy $U(BN) = [E_{\text{total}}(BN) - \mu_B n_B - \mu_N n_N]/(n_B + n_N)$ on the tube curvature. (Chemical potentials are taken

TABLE III. Predicted elastic constants for C_2F nanotubes from periodic PBE/3-21G calculations.

Tube	$d^2E/d\epsilon^2$	C,J/m^2	ν	$\frac{1}{6}d^3E/d\epsilon^3$	L	Shortest F-F
(4,4)	58.4	345		−1650	2.492	2.731
(10,10)	53.8	323		−1780	2.501	2.564
planar (∞,∞)	54.5	328	0.039	−1890	2.513	2.393

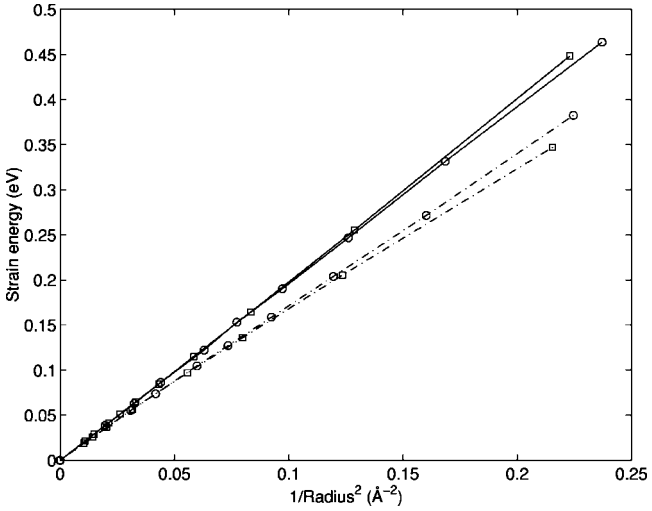

FIG. 1. Curvature strain energy for carbon and BN tubes as a function of the square of their inverse radius. ○ and solid lines represent data for $(n,0)$ carbon tubes; □ and solid lines represent data for (n,n) carbon tubes; ○ and dashdotted lines represent data for $(n,0)$ BN tubes; □ and dashdotted lines represent data for (n,n) BN tubes.

from flat *BN* sheet, and $n_N = n_B$.) In Fig. 1, the nonlinearity of the dependence of $U(BN)$ on $1/R^2$ is evident. The best formal fit of energies to a power law yields $a = 1.94$, $\tilde{D} = 3.20$ for (n,n) BNNT's with $n = 5-40$, and $a = 1.95$, $\tilde{D} = 3.30$ when fitting for $n = 10-40$. Assuming that the dependence is approximately quadratic, we compute $D = 3.62$ eV Å^2/atom for (10,10) BNNT ($R = 7$ Å). This coefficient D is directly comparable to the flexural rigidity values for carbon. The subquadratic dependence of the energy on the radius for BNNT's is likely a consequence of the BNNT's buckling, with B atoms displaced toward the tube axis and N atoms pushed outwards. The plot of the degree of buckling versus the tube radius is shown in Fig. 2. Similar to

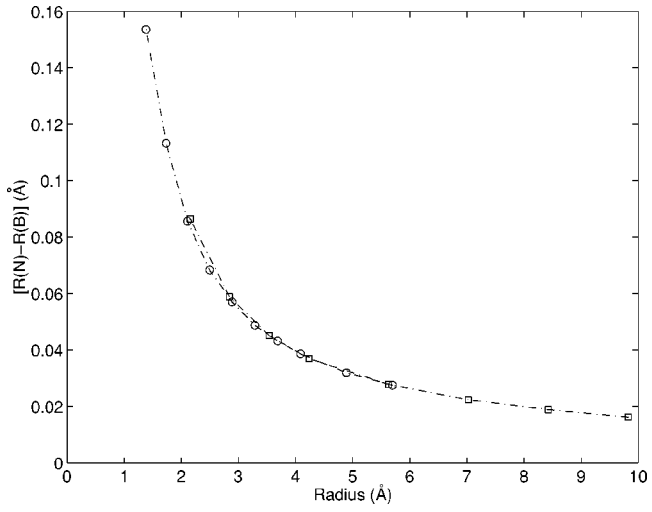

FIG. 2. Buckling in the BN tube equilibrium structures versus the tube radius. ○ represent data points for $(n,0)$ tubes; □ represent data points for (n,n) tubes.

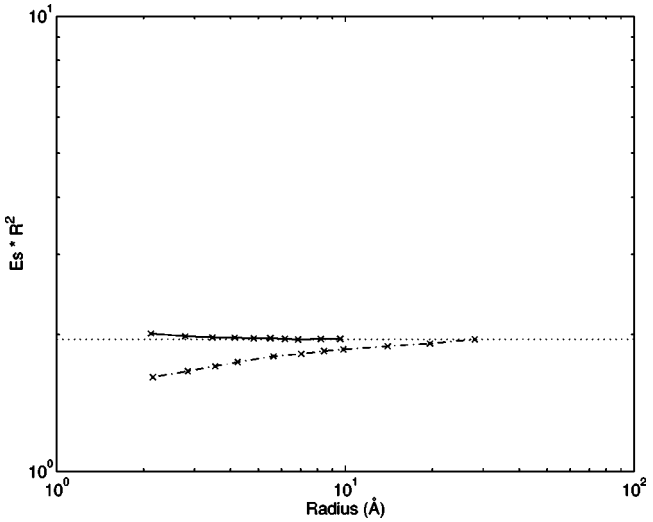

FIG. 3. Log-log plot of $[UR^2]$ versus the tube radius. Solid lines represent data points for (n,n) carbon tubes; dashdotted lines represent data for (n,n) BN tubes. The dotted line indicates asymptotic behavior of the $[U \cdot R^2]$ for carbon tubes.

the strain energy itself, the buckling does not depend on the BNNT type $[(n,0)$ or $(n,n)]$ and is a function of the tube radius only. Using log-log fits, we established that for large diameter tubes, the degree of buckling is sublinear with respect to the curvature $1/R$, with $\delta R_{BN} \approx 0.2\%$ for one of the largest ($R = 10$ Å), and $\delta R_{BN} \approx 10\%$ for the smallest tubes ($R = 1.5$ Å). Comparing the degree of buckling predicted by our DFT calculations with that obtained via a tight-binding scheme (TB),[27] it appears that in our case the radius difference is smaller, by about 20–30 %.

More interestingly, for smaller tubes of matching radius, the strain energy for CNT's is larger than for BNNT's, while for very large tubes the opposite is likely to be true. To examine this issue in more detail, we carried out calculations for large BN tubes [(20,20), (28,28), (40,40)]. The log-log plot of UR^2 on tube radius for CNT's and BNNT's of (n,n) type is shown in Fig. 3. The slope of the line going through BN tube data points is smaller than for carbon tubes, indicating that $a < 2.0$. It is also evident that the lines for CNT's and BNNT's cross and the strain energy for BN tubes becomes larger than for carbon ones at about $n = 40$.

C. C_2F (n,n) tubes

Analogously to CNT and BNNT's, the formation energy is computed per node of hexagonal network (that is per each C in the tubule) as $E(C_2F) = [E_{\text{total}}(C_2F) - \mu_C n_C - \mu_F n_F]/n_C$, where μ_F is defined as the fluorine atom energy in a free molecular F_2, and μ_C is carbon energy in graphene sheet as previously. We note that $E(C_2F)$ is the same as $1/2\, E_2$ found in Table IV. In contrast to pure *C* and *BN* tubes, the strain energy $U(C_2F) = E(C_2F) - E_{\text{flat}}(C_2F)$ does not fit the $\propto 1/R^2$ dependence. On the other hand, a formation energy $E(C_2F)$ versus curvature $(1/R)$ dependence is more revealing as it shows approximately parabolic dependence with a minimum distinctly away from zero curvature, Fig. 4. (For comparison purposes, Fig. 4 includes corresponding plots for

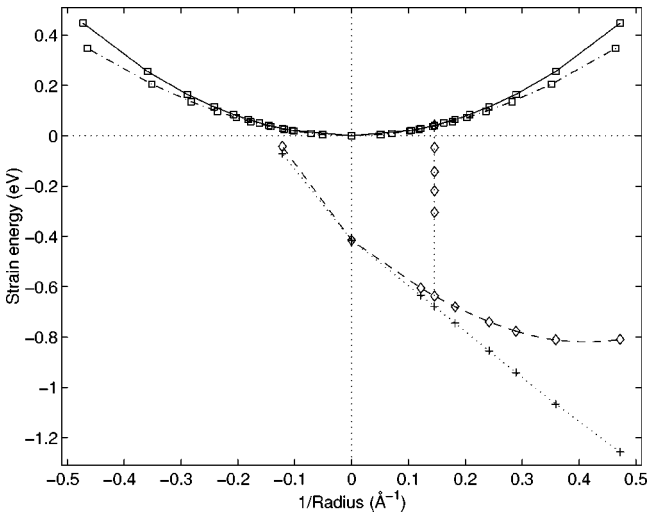

FIG. 4. Strain energy for carbon, BN and C_2F tubes as a function of their curvature (inverse radius). □ and solid line represent data for (n,n) CNT's; □ and dashdotted line represent data for (n,n) BNNT's; ◇ and dashed line represent $E(C_2F)$ $[1/2E_1]$ for F-CNT's; + and dotted line represent 1/2 E_2 for F-CNT's; ◇ and vertical dotted line indicates fluorination energy per carbon in F_y-(10,10) where $y=1-4$.

CNT's and BNNT's.) With this shift taken into account, the strain energy curve looks again as characteristic parabolic function $U(C_2F)=\frac{1}{2}\ D_{CF}(1/R-1/R_{eq})^2$. Remarkably, the energy minimum corresponds to very large spontaneous curvature $1/R_{eq}=0.46$ (Å^{-1}), that is to the tubes of (4,4) and even (3,3) type with the diameters as small as near 5 Å. Cross sections of (6,6), (5,5), (4,4), and (3,3) tubes are distinctly polygonal as shown in Figs. 5(a), 5(b), 5(c), 5(d). The formally defined value of the flexural rigidity is then $D_{CF}=3.96$ eV A^2/atom. These $1/R_{eq}$ and D_{CF} values were estimated by fitting energies for three larger diameter F-CNT's: (8,8), (10,10), (12,12). It is quite interesting to note that D coefficients for F-CNT's and CNT's are almost the same, and as a result, the difference between the two parabolas representing the CNT fluorination energy is close to a straight line (same as 1/2 E_1 in Table IV).

The significant spontaneous equilibrium curvature caused by unilateral fluorination is a strong manifestation of asymmetry of the formed C_2F layer. Another measure of this asymmetry is a nonvanishing first derivative of energy with respect to curvature in the vicinity of zero, which is a finite internal bending torque in a flat fluorinated sheet. The direction of this torque and the sign of the resulting equilibrium curvature correspond to "fluorine repulsion," making the fluorination on a convex side much more favorable than on a concave side. Tubes (12,12) with all-outside and all-inside fluorine are shown in Figs. 5(e) and 5(f), while the difference in their energies is evident from Fig. 4. We will see further that the main cause of the curvature is a locally induced angle, a "pinch" in the underlying carbon network, rather than a repulsion between the neighboring F-zigzag rows.

Overall, for the monatomic shells considered in this work, we observe three types of behavior with respect to flexing. The response of the isotropic carbon sheet is symmetric with respect to positive and negative curvature, and the dependence of the strain energy on curvature is quadratic. For an asymmetric C_2F sheet, the energy dependence is linear for small flexing and attains a minimum for high spontaneous curvatures. The BN sheet is an intermediate material between graphite and fluorinated graphite. While the BN strain energy curve is symmetric with respect to the zero curvature line, the dependence is between linear and quadratic. This is an indication of induced asymmetry, likely due to buckling in the BN tubes.

V. LOCALIZATION OF STRAIN IN FLUORINATED (n,n) TUBES

The energy minimum near the (4,4) F-CNT [Fig. 5(c)] prompted us to look at larger square (or other polygonal) structures that have four fluorine chains and rows of sp^2 carbon between them. Adding eight fluorine atoms to the unit cells of (6,6), (8,8), and (10,10), we have obtained structures with the varying stoichiometries C_3F, C_4F, C_5F, respectively. (10,10) tubes with four and five fluorine chains are shown in Figs. 6(a) and 6(b). For both these examples we observe a distinctly polygonal cross section with rows of sp^2 carbon forming bands of graphitelike material with very little visible deviation from planarity.

The data indicating the stability of the fluorinated tubes is shown in Table IV. Energy E_1 $(E_1=[E_{\text{total}}(C_2F)-E_{CNT}n_C-\mu_F n_F]/n_F)$ describes how stable the fluorinated tube is compared to the carbon in the corresponding pristine CNT and fluorine in F_2. In addition, energy E_2 $(E_2=[E_{\text{total}}(C_2F)-\mu_C n_C-\mu_F n_F]/n_F)$ describes the relative energy of a fluorinated tube with respect to carbon in a graphene and the fluorine in F_2. Therefore, E_2 is a more systematic measure of the comparable stability of various isomers. Due to the positive strain energy in SWNT's and consequently higher energy of the formal reactants, E_1 is always lower than E_2 except for the one side fluorinated graphene sheet, where these values are the same. In F-CNT's of C_2F stoichiometry the most energetically favorable are tubes of the smallest radius, where in (3,3) F-CNT the E_1 energy per fluorine reaches values as low as -2.51 eV, and E_2 reaches -1.62 eV. In contrast, the stabilization energies for the all-inside (12,12) SWNT is extremely small, with E_1 being -0.14 eV and E_2 being -0.09 eV. Such high values are partially due to the substantial repulsion of fluorine atoms located too close to each other inside the tube. We have already encountered E_1 and E_2 in the previous section while discussing Fig. 4.

For square tubes of varying stoichiometry, the energy with respect to carbon in graphene (E_2) slightly increases with increasing tube size and converges to -1.51 eV per fluorine. The fact that the latter value is very similar for all square tubes quantifies our statement that the sp^2 carbons between fluorinated corners are pretty much the same as carbons in a graphene sheet. Another interesting observation is that for all square tubes, the E_2 values are lower than for F-CNT of C_2F composition, for example in the (6,6) tube (-1.56 eV versus -1.48 eV). So, if reaction kinetics per-

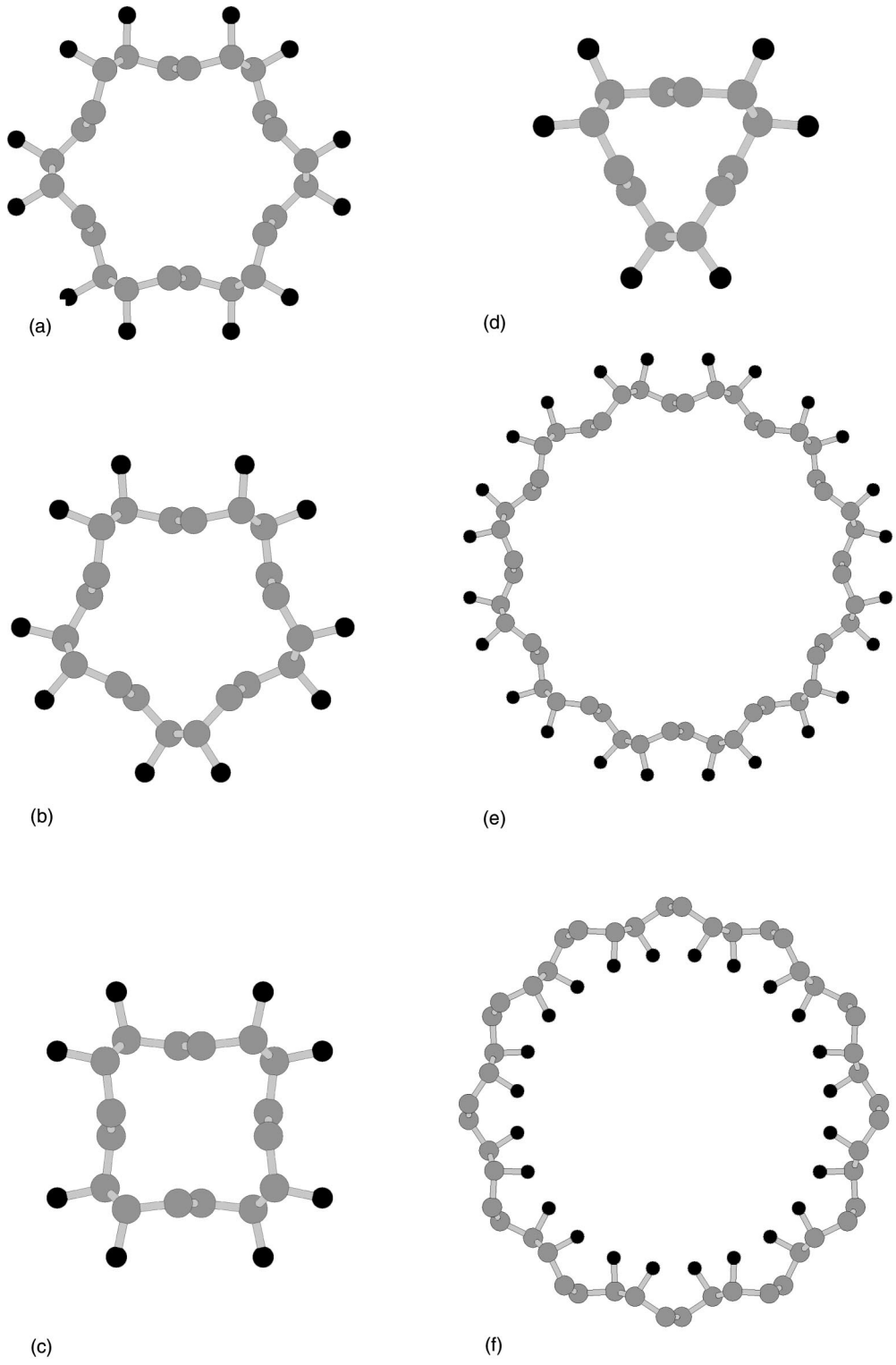

FIG. 5. Geometries of the fluorinated (n,n) carbon tubes of C_2F stoichiometry. (a) F-(6,6); (b) F-(5,5); (c) F-(4,4); (d) F-(3,3); (e) F-(12,12); (f) F_i-(12,12).

mit, fluorination of pristine carbon tubes might produce square tubes in cases when the carbon/fluorine ratio is small. Formation of square tubes might proceed via a consequent addition of fluorine chains to the pristine tube [Figs. 7(a), 7(b), 7(c)]. In order for such a scheme to work in practice, two assumptions should be true, first that fluorine atoms prefer to add in chains along the tube, and second, that such fluorine chains prefer to add in the area of the tube with the largest mechanical strain. Using the (10,10) tube as an example, we can quantify the energetics of such a mechanism. Adding just one chain of fluorines to the (10,10) SWNT, the energy per fluorine E_1 (-1.76 eV) is substantially smaller

TABLE IV. F-CNT fluorination energies and Fermi level in eV. F-(x,x) are outside fluorinated tubes of C_2F stoichiometry, F_i-(12,12) is the inside fluorinated (12,12) of C_2F stoichiometry, F_4-(x,x) are square tubes, and F_n where $n=1-3$ are fluorinated tubes shown in Fig. 7. For partially fluorinated tubes F_n, the energy per new fluorine atom relative to the previous structure is shown in parentheses.

Tube	E_1	E_2	E_{Fermi}
F-(3,3)	−2.51	−1.62	−6.62
F-(4,4)	−2.13	−1.62	−6.80
F-(6,6)	−1.71	−1.48	−6.95
F-(8,8)	−1.49	−1.36	−6.99
F-(10,10)	−1.36	−1.27	−7.00
F-(12,12)	−1.27	−1.21	−7.01
F-(∞,∞)	−0.83	−0.83	−5.86
F_i-(12,12)	−0.14	−0.09	−4.55
F-(4,4)	−2.13	−1.62	−6.80
F_4-(6,6)	−1.90	−1.56	−6.50
F_4-(8,8)	−1.79	−1.53	−6.31
F_4-(10,10)	−1.73	−1.52	−6.20
F_4-(12,12)	−1.69	−1.52	−6.08
F_4-(14,14)	−1.66	−1.51	−6.00
F_1-(10,10)	−1.76	−0.94	−5.17
F_2-(10,10)	−1.84(−1.92)	−1.43	−5.61
F_3-(10,10)	−1.73(−1.51)	−1.46	−5.85
F_4-(10,10)	−1.73(−1.73)	−1.52	−6.20

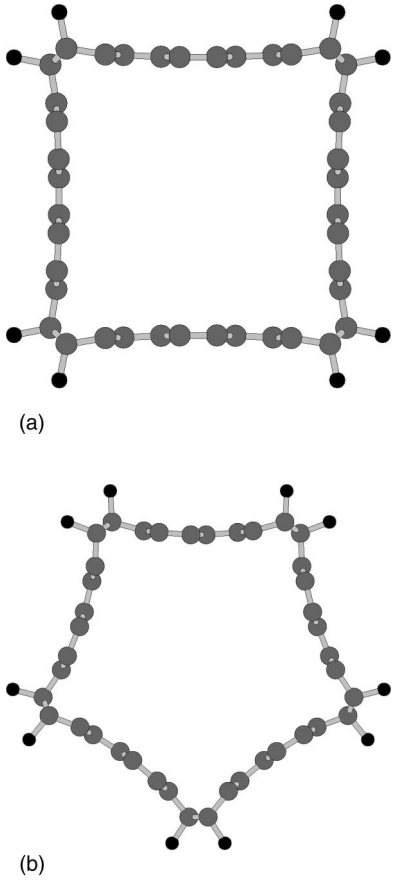

FIG. 6. Geometries of the polygonal fluorinated carbon tubes. (a) square F_4-(10,10); (b) pentagonal F_5-(10,10).

than E_1 for the entirely fluorinated F-(10,10) tube (−1.36 eV). The same is true for all intermediates that lead to a square tube. So, from a thermodynamical perspective, fluorine chains would like to attach in areas where there are no other fluorine chains nearby.

The cross sections of all the low-fluorinated structures (where F is attached along the axially directed zigzag motifs) permit simple continuum elasticity interpretation. They essentially represent elastic sheets constrained by appropriate boundary conditions at the F junctions, and belong therefore to the class of Euler's ELASTICA curves. This again confirms that uniform domains in nanotubes can be quite well described by macroscopic elasticity theory. Figure 8 shows such curve for a $C_{20}F$ tube [F_1-(10,10)]. It is matched to form a closed loop with a single F junction, inserting an angle $\phi=71°$. The value of ϕ is established in a complete relaxation of a "corner" structure ($HC\cdots CCF_2C\cdots CH$), hydrogen-terminated in order to eliminate the torque present in a closed loop [Fig. 7(d)]. The fact that observed deviations from 71° in different polygonal shapes are very small demonstrate its relative stiffness compared to compliant extensive carbon sheet. Notably, addition of an F_2 group (linear motif) to a flat graphite sheet changes its global geometry. This presents a peculiar chemomechanical coupling where

TABLE V. Summary for computed elastic constants for C, BN, and C_2F lattices.

	C	BN	C_2F
2D properties			
in-plane stiffness C, N/m	345	271	328
(Y_{bulk}, Gpa)	(1029)	(810)	(979)
flexural rigidity D, eV	1.46	1.29	1.49
shear modulus G	150	112	158
Poisson ratio ν	0.149	0.211	0.039
3D properties			
shell thickness h_s, Å	0.894	0.936	0.933
Young modulus Y_s, Gpa	3859	2901	3515
shell shear modulus G_s	1679	1198	1692
surface density ρ_s, mg/m^2	0.749	0.736	1.342
frequencies for (10,10) tube			
f_{ext}, cm^{-1}	168	148	121
f_{axial}, cm^{-1}	110	93	84
f_{flex}, cm^{-1}	17.0	15.3	12.8

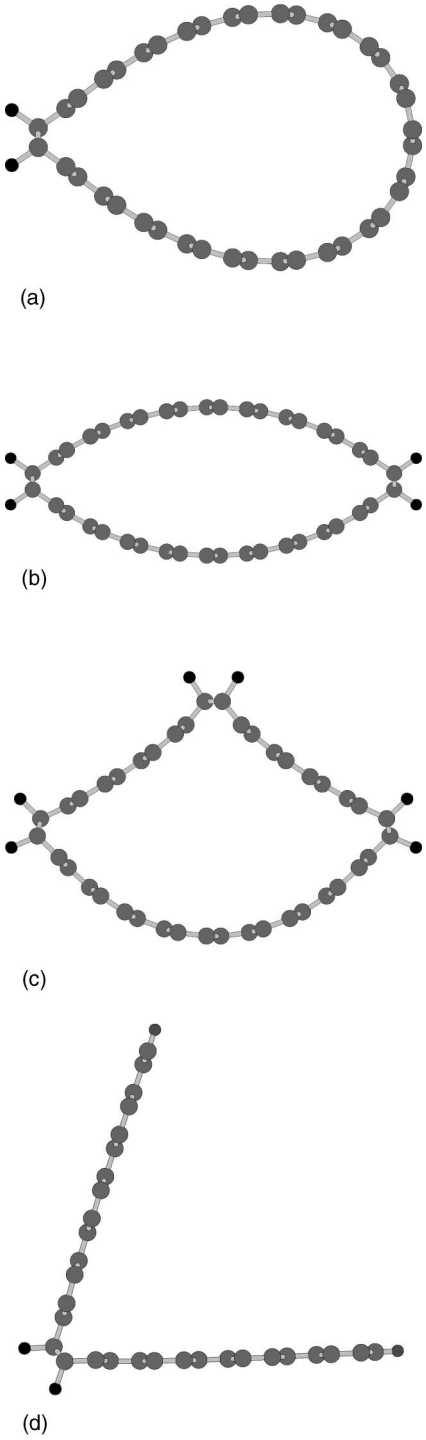

FIG. 7. Geometries of the fluorinated (10,10) carbon tubes with low fluorine content and the unconstrained fluorinated angle. (a) F_1-(10,10); (b) F_2-(10,10); (c) F_3-(10,10); (d) unconstrained fluorinated angle.

chemical energy of fluorination can be transformed into mechanical work of the sheet bending.

VI. CONCLUSIONS

We conclude by emphasizing the applicability of the elastic shell model to the objects of molecular size. This significant simplification of description can be achieved, provided that the parameters of the shell are accurately determined *ab initio*, and allows one to employ the well established relationships for macroscopic shells. Table V summarizes some of the results for C, BN, and C_2F lattices, omitting the minor differences discussed in the text (e.g., for different tube radii and chiralities). The first block presents the formal two-dimensional shell in-plane stiffness C, flexural rigidity D, and the shear modulus $G=C/[2(1+\nu)]$. The second line in parenthesis supplies the bulk Young's modulus Y_{bulk} of a 3D stack of layers spaced at 3.35 Å apart from each other, along the plane; we include it here for the sake of convenient comparison with graphite. We also include the values of two-dimensional mass density ρ_s for the three materials. In the second block we define an effective material shell, which is most common in the studies of macroscopic shells elasticity, vibrations and nonlinear buckling. The finite thickness and the effective Young's modulus is assigned based on Eq. (4). We note that a very small thickness combines with a very high Young's modulus to provide a consistent representation (the values here differ of course from those based on the empirical classical potential, Ref. 8). In the bottom section we present the frequencies of several basic vibrations calculated from the shell parameters (the speed of light c is included to convert to spectroscopic inverse centimeters units). Extension-breathing mode A_{1g} (circular shape preserved, radial oscillation)

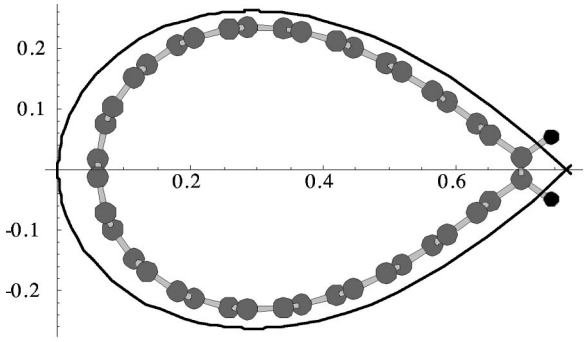

FIG. 8. Overlay of the Euler's *Elastica* curve and the F_1-(10,10) tube of $C_{20}F$ stoichiometry.

$$f_{\text{ext}}=\frac{1}{2\pi cR}\sqrt{\frac{C}{(1-\nu^2)\rho_s}}. \tag{5}$$

Axial shear mode E_{1g} (relative axial displacement of the opposite sides of the cylinder)

$$f_{\text{axial}}=\frac{1}{2\pi cR}\sqrt{\frac{C}{2(1+\nu)\rho_s}}. \tag{6}$$

The softest flexural-circumferential mode E_{2g} (flattening of the cylinder) has frequency

$$f_{\text{flex}} = \frac{h_s}{4\pi c R^2}\sqrt{\frac{12C}{5\rho_s(1-\nu)}}. \quad (7)$$

The presented frequencies are for the (10,10) tubes and for an arbitrary radius that obviously scales as $f(d) = f(10,10) \times 7$ Å$/R$. The values presented here can be compared with the previously reported measurements and atomic-model calculations (e.g., Ref. 29). A well-quantified shell model allows one to go beyond linear analysis in the assessment of stability, buckling and strength limits of the shell-based structures.

ACKNOWLEDGMENTS

This work was supported by the NSF (Grant No. CHE 9982156), DMR (Grant No. 0073046) (K.N.K. and G.E.S.), and Air Force (Contract No. F33615-98-C-5435) (B.I.Y.).

[1] M.S. Dresselhaus, G. Dresselhaus, and P.C. Eklund, *Science of Fullerenes and Carbon Nanotubes* (Academic Press, San Diego, 1996), p. 965.
[2] S. Iijima, Nature (London) **354**, 56 (1991).
[3] N.G. Chopra, R.J. Luyken, K. Cherrey, V.H. Crespi, M.L. Cohen, S.G. Louie, and A. Zettl, Science **269**, 966 (1995).
[4] E.T. Mickelson, C.B. Huffman, A.G. Rinzler, R.E. Smalley, R.H. Hauge, and J.L. Margrave, Chem. Phys. Lett. **296**, 188 (1998).
[5] E. Bengu and L.D. Marks, Phys. Rev. Lett. **86**, 2385 (2001).
[6] J. Tersoff and R.S. Ruoff, Phys. Rev. Lett. **73**, 676 (1994).
[7] D.J. Srolovitz, S.A. Safran, M. Homyonfer, and R. Tenne, Phys. Rev. Lett. **74**, 1779 (1995).
[8] B.I. Yakobson, C.J. Brabec, and J. Bernholc, Phys. Rev. Lett. **76**, 2511 (1996).
[9] B.I. Yakobson and P. Avouris, *Mechanical Properties of Carbon Nanotubes, in Carbon Nanotubes*, edited by M.S. Dresselhaus and P. Avouris (Springer-Verlag, Berlin, 2001), pp. 287–327.
[10] L.D. Landau and E.M. Lifshitz, *Elasticity Theory*, 3rd ed. (Pergamon, New York, 1986), p. 187.
[11] K.N. Kudin and G.E. Scuseria, Phys. Rev. B **61**, 16 440 (2000).
[12] GAUSSIAN 99, Development Version (Revision B.08+), M. J. Frisch, G. W. Trucks, H. B. Schlegel, G. E. Scuseria, M. A. Robb, J. R. Cheeseman, V. G. Zakrzewski, J. J. A. Montgomery, R. E. Stratmann, J. C. Burant, S. Dapprich, J. M. Millam, A. D. Daniels, K. N. Kudin, M. C. Strain, O. Farkas, J. Tomasi, V. Barone, B. Mennucci, M. Cossi, C. Adamo, J. Jaramillo, R. Cammi, C. Pomelli, J. Ochterski, G. A. Petersson, P. Y. Ayala, K. Morokuma, D. K. Malick, A. D. Rabuck, K. Raghavachari, J. B. Foresman, J. V. Ortiz, Q. Cui, A. G. Baboul, S. Clifford, J. Cioslowski, B. B. Stefanov, G. Liu, A. Liashenko, P. Piskorz, I. Komaromi, R. Gomperts, R. L. Martin, D. J. Fox, T. Keith, M. A. Al-Laham, C. Y. Peng, A. Nanayakkara, M. Challacombe, P. M. W. Gill, B. Johnson, W. Chen, M. W. Wong, J. L. Andres, C. Gonzalez, M. Head-Gordon, E. S. Replogle, and J. A. Pople (Gaussian, Inc., Pittsburgh, PA, 2000).
[13] J.P. Perdew, K. Burke, and M. Ernzerhof, Phys. Rev. Lett. **77**, 3865(E) (1996); **78**, 1396(E) (1997).
[14] L. Greengard and V. Rokhlin, J. Comput. Phys. **73**, 325 (1987).
[15] K.N. Kudin and G.E. Scuseria, Chem. Phys. Lett. **283**, 61 (1998).
[16] K.N. Kudin and G.E. Scuseria, Chem. Phys. Lett. **289**, 611 (1998).
[17] K.N. Kudin and G.E. Scuseria, J. Chem. Phys. **111**, 2351 (1999).
[18] K.N. Kudin and G.E. Scuseria, Phys. Rev. B **61**, 5141 (2000).
[19] K.N. Kudin, G.E. Scuseria, and H.B. Schlegel, J. Chem. Phys. **114**, 2919 (2001).
[20] N. Hamada, S. Sawada, and A. Oshiyama, Phys. Rev. Lett. **68**, 1579 (1992).
[21] X. Blase, L.X. Benedict, E.L. Shirley, and S.G. Louie, Phys. Rev. Lett. **72**, 1878 (1994).
[22] A. Rubio, J.L. Corkill, and M.L. Cohen, Phys. Rev. B **49**, 5081 (1994).
[23] X. Blase, J.-Ch. Charlier, A. De Vita, and R. Car, Appl. Phys. A: Mater. Sci. Process. **68**, 293 (1999).
[24] K.N. Kudin, H.F. Bettinger, and G.E. Scuseria, Phys. Rev. B **63**, 045413 (2001).
[25] H. F. Bettinger, K. N. Kudin and G. E. Scuseria, J. Am. Chem. Soc. (to be published).
[26] D. Sanchez-Portal, E. Artacho, J.M. Soler, A. Rubio, and P. Ordejon, Phys. Rev. B **59**, 12 678 (1999).
[27] E. Hernandez, C. Goze, P. Bernier, and A. Rubio, Phys. Rev. Lett. **80**, 4502 (1998).
[28] J. Kurti, G. Kresse, and H. Kuzmany, Phys. Rev. B **58**, 8869 (1998).
[29] A.M. Rao, E. Richter, S. Bandow, B. Chase, P.C. Eklund, K.A. Williams, S. Fang, K.R. Subbaswamy, M. Menon, A. Thess, R.E. Smalley, G. Dresselhaus, and M.S. Dresselhaus, Science **275**, 187 (1997).